Electronic Supplementary Information (ESI)

One-step synthesis of benzothiadiazole-based nonbranching functionalized covalent organic framework and its application in efficient removal of Hg^{2+}

Guizhen Li, ‡ Yuanzhe Cao, ‡ Bo Zhang, Qiang Zhang, Yingyuan Hu* and Xin Zhao*

School of Chemistry and Life Sciences, Suzhou University of Science and Technology, Suzhou, Jiangsu, 215009, China.

Corresponding author: Xin Zhao and Yingyuan Hu, Address: School of Chemistry and Life Sciences, Suzhou University of Science and Technology, 215009 Suzhou, China, Email: zhaoxinsz@usts.edu.cn, huyy@usts.edu.cn

Table of Content

Section S1. Materials and methods

1,3,6,8-tetrakis(4-formylphenyl) pyrene, p-Phenylenediamine and S_8 were purchased from Leyan. Acetic acid（HOAc, 99%）, dimethyl sulfoxide (DMSO, 98%), 1,2-dichlor-obenzene (o-DCB, 99%), n-butyl alcohol (n-BuOH, 99%), tetrahydrofuran (THF, 99%) were purchased from Mackiln. All standard ion solutions were purchased from the General Research Institute of Nonferrous Metals in Beijing.

1. PXRD: Powder X-ray diffraction (PXRD) data were recorded on a Bruker AXS D_8 ADVANCE diffractometer using Cu K_α (λ = 1.5406 Å) at 1600 W power (40 kV, 40 mA) from 2θ = 2.5°- 30° in 0.034° increments, with 1s exposure per step.

2. FT-IR: Fourier transform infrared (FT-IR) data were recorded on a PerkinElmer Spectrum 400 spectrometer in the wavelength range 4000 - 500 cm^{-1}.

3. ^{13}C NMR: cross-polarization magic-angle spinning (CP-MAS) NMR experiments were tested on a Bruker WB Avance II 400 MHz NMR spectrometer. Using a three-channel, 4 mm probe. Cross-polarization with Magic Angle Spinning (CP-MAS) was used to acquire ^{13}C data at 100 MHz. The spectral width of the pulse sequence was 35 kHz, the 1H excitation pulse was 3 μs and the contact time was 3.5 ms. High power double pulse phase modulation (TPPM) ^{1}H decoupling was used with a decoupling frequency of 80 khz, a cycle delay of 4 s and a sample spinning rate of 10 kHz.

4. BET: N_2 adsorption and desorption isotherms were carried out using a Micrometrics ASAP 2460 analyses at 77 K. The samples were degassed at 323 K for 8 h prior to measurement. Prior to measurement, samples were degassed at 323 K for 8 h. The specific surface area was calculated from the adsorption data using the Brunauer-Emmett-

Teller (BET) method. Pore size distribution data were calculated based on a Non-local density flooding theory (NLDFT) model.

5. SEM: Scanning electron microscope (SEM) was examined using the instrument SIGMA 300 at an accelerating voltage of 5 kV.

6. TEM, EDS: Use JEM-2100F for High-resolution transmission electron microscopy (HRTEM) test, which is equipped with a JEM-2010HR-Vantage typed energy spectrometer for Energy-dispersive X-ray spectroscopy (EDS). Samples were coated with gold and dispersed over a slice of conductive adhesive adhered to a copper platform sample holder. Images of HRTEM were acquired using a high-resolution CCD camera (2048 × 2048 pixels).

7. TGA: Thermogravimetric analyses of the samples was carried out using a TA Instruments thermalbalance TGA 55 thermal gravimetric analyzer with the samples placed in an alumina crucible under a nitrogen atmosphere. The samples were heated at a rate of 10° min^{-1} over a temperature range of 25 - 600°C.

Section S2. Synthesis of TPS-COF

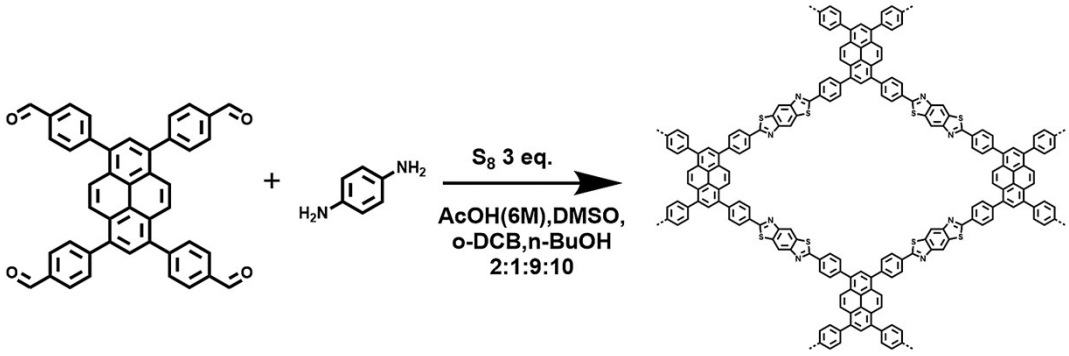

The material was solvothermally synthesized using a modified literature procedure, wherein 1,3,6,8-tetrakis(4-formylphenyl)pyrene-TFPPA (20 mg, 0.032 mmol), p-Phenylenediamine-PD (6.9 mg，0.064 mmol) and S_8 (12.1 mg, 0.38 mmol)were added into a 10 mL Schlenk tube and dissolved in the mixture of o-DCB/n-BuOH (9/10, 0.95 mL), the mixture was mixed by sonication, then oxidizing reagent DMSO (0.05 mL) and 6 M acetic acid (0.1 mL) catalytic solution were added, respectively. Sonicated and degassed by three freeze-pump-thaw cycles, the mixture was reacted in an infrared oven at 393 K for 72 h. The crude product was washed and filtered three times using tetrahydrofuran and extracted in tetrahydrofuran, acetone and ethanol to obtain the orange powder. The powder was dried overnight at 80 °C under vacuum to give a final product in 94 % yield.

Table. S1. Condition selection

Solvent	Solvent 2	Volume	Catalysts	Oxidizing	Time	Temp	Crystallinity
o-DCB	EtOH	9:10 (0.95 mL)	6 M	DMSO	3 d	120 °C	Semicrystalline
Dioxane	Mesitylene	9:10 (0.95 mL)	6 M	DMSO	3 d	120 °C	Crystalline
DMAc	Mesitylene	9:10 (0.95 mL)	6 M	DMSO	3 d	120 °C	Crystalline
THF	DMAC	9:10 (0.95 mL)	6 M	DMSO	3 d	120 °C	Semicrystalline
o-DCB	n-BuOH	9:10 (0.95 mL)	6 M	DMSO	3 d	120 °C	Crystalline

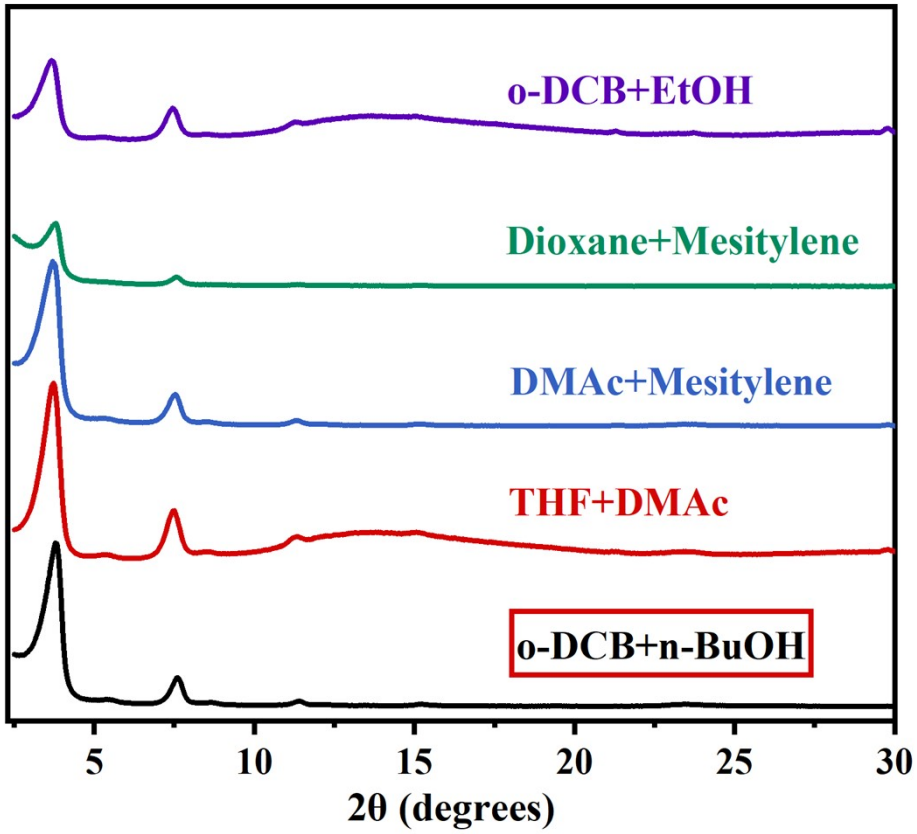

Fig. S1. Condition selection PXRD for TPS-COF.

Section S2. Comparison data reported for COFs materials used for Hg^{2+} adsorption

Table. S2. Comparison data reported for COFs materials used for Hg^{2+} adsorption [*]

COFs	BET surface $m^2\ g^{-1}$	Q_e $mg\ g^{-1}$	Time	Nonbranching (×) or branching (√) functionalized	Reference
COF--SH	235.00	1282.60	30 min	√ (-SH, -OH)	[S1]
COF-LZU1	230.00	113.00	30 min	√ (Ag)	[S2]
M-COF-SH	181.50	383.00	10 min	√ (-SH)	[S3]
TPB-DMTP-COF-SH	291.00	4395.00	2 min	√ (-SH)	[S4]
TAPB-BMTTPA-COF	1934.00	734.00	5 min	√ (-SMe)	[S5]
ACOF	296.00	175.00	5 min	× (C=O)	[S6]
TFPPy-CHYD COF	763.00	758.00	5 min	× (-NH)	[S7]
Pyridine-COF	348.50	99.50	60 s	× (Pyridine）	[S8]
COF-S-SH	1152.00	1350.00	10 min	√ (-S-, -SH)	[S9]
COF-S-SH COF-OH-SH	814.80 720.30	586.30 535.50	60 min	√ (-S-, -SH) √ (-OH, -SH)	[S10]
T-COF	328.00	1815.00	15 min	× (N=N)	[S11]
COF-S-SH	234.00	255.80	50 min	√ (-S-, -SH)	[S12]
JNU-3	420.00	960.00	10 s	× (Thiourea)	[S13]
TpTSC	205.00	1035.00	10 min	× (Thiourea)	[S14]

BBT-FCOF	32.91	4987.00	--	× (Thiazole)	[S15]
TP-EDDA COF	1183.00	718.00	10 min	× (Dispersed S)	[S16]
POFct-1	167.19	216.41	720 min	√ (-NH^+, -O^-)	[S17]
TPS-COF	1564.00	1040.00	10 min	× (Thiazole)	This work

[*] As can be seen from the available data, there is no shortage of published materials for COFs with high Hg^{2+} adsorption, but the specific surface area or crystallinity has been sacrificed in order to achieve high functionality. Furthermore, most of the available studies are based on the modification of functionalized branched chains to achieve the goal, which is a cumbersome and expensive synthesis process.

Section S3. Simulation calculation

The molecular models of the COFs were constructed using the Materials Studio (version 2020) program. The geometry was initially optimized using the MS Forcite module, with the Forcefield parameter chosen as Universal and the algorithm using Quasi-Newton. First, we downscaled the lattice symmetry to P1, inserted the optimized monomer into the empty cell, omitted the redundant atoms, filled in the structural connection points, and raised the symmetry up to the corresponding space group to produce the coarse structure of the COF (AA stacking). The lattice model is then geometrically optimized (Geometry Optimization) using the MS Forcite Molecular Dynamics module to obtain optimized lattice parameters, and the optimized structures of the COFs show distorted arrangements. Finally, using the Reflex Plus module, the corresponding PXRD patterns were simulated by applying the diffraction simulation function (Powder Diffraction) number. The R_{wp} and R_p values were converged as far as possible (taking into account the broadening of the spectral lines due to grain size and lattice strain). In addition, a staggered arrangement (AB stacking) of TPS-COF was constructed with alternate stacking cell offsets a/2 and b/2, and the above steps were repeated to complete the structural optimization and PXRD pattern simulation.

Table. S3. AA stacked atomic coordinates

Atomistic coordinates for the AA-stacking mode of TPS-COF optimized using Forcite method (space group C2/M (12), a = b = 34.48120 Å; c = 3.67057 Å, α = β = γ = 90 °).

Atom	x/a	y/b	z/c
C1	105.014	-77.702	2.571
C2	105.02	-85.009	2.568
C3	104.961	-86.245	3.237
C4	106.066	-87.104	3.253
C5	107.264	-86.738	2.614
C6	107.343	-85.478	1.999
C7	106.231	-84.636	1.958
C8	106.224	-78.073	1.96
C9	107.335	-77.229	1.999
C10	107.255	-75.97	2.614
C11	106.057	-75.605	3.253
C12	104.954	-76.465	3.239
C13	108.397	-75.026	2.519
C14	108.406	-87.681	2.518
N15	109.582	-75.409	1.989
S16	108.278	-73.359	2.964
S17	108.289	-89.347	2.971

C18	109.882	-89.522	2.41
C19	110.42	-88.345	1.922
N20	109.588	-87.302	1.98
C21	112.45	-73.232	1.414
C26	111.91	-72.053	1.894
N27	110.616	-90.711	2.406
C28	111.914	-90.659	1.888
S29	112.452	-89.483	1.398
S30	111.717	-88.294	1.402
C31	112.748	-91.701	1.836
N32	113.932	-91.32	1.302

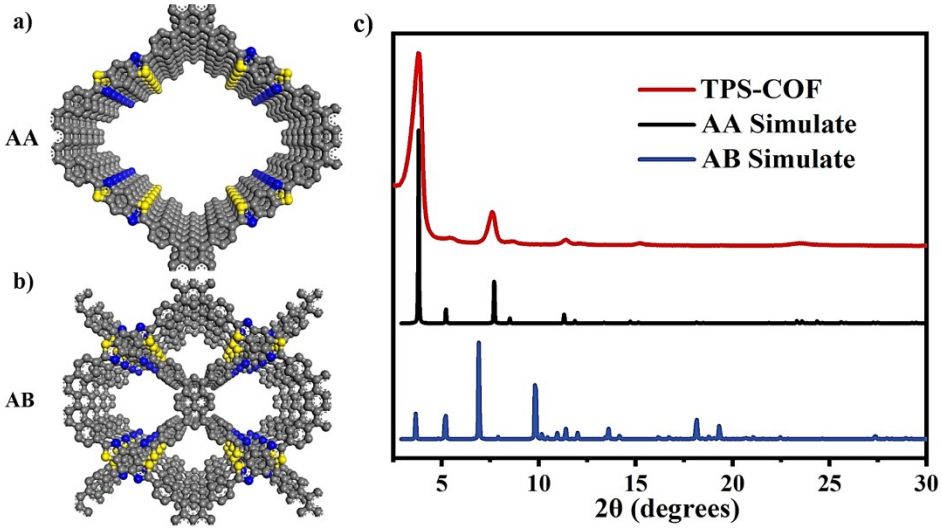

Fig. S2. Simulation of the TPS-COF stacking model (a) AA stacking model for TPS-COF. (b) AB stacking model for TPS-COF. (c) Experimental, AA and AB PXRD stacking models of TPS-COF.

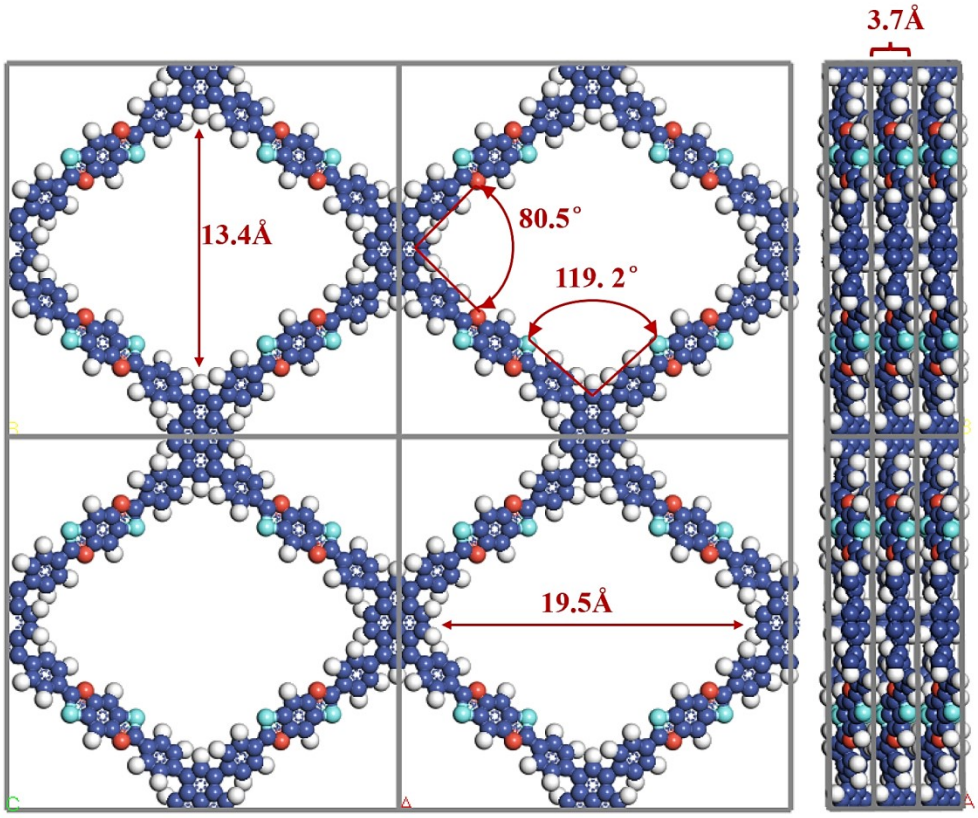

Fig. S3. TPS-COF model for Forcite force field optimization simulation.

Section S4. Characterization

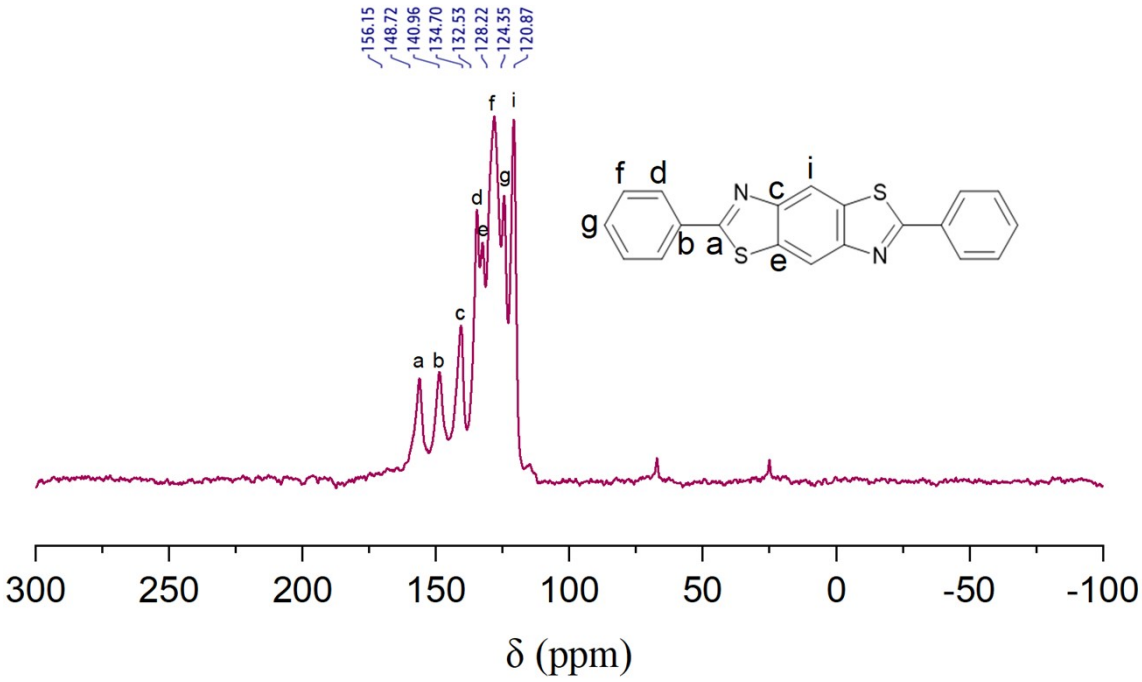

Fig. S4. Solid-state ^{13}C NMR spectra of TPS-COF.

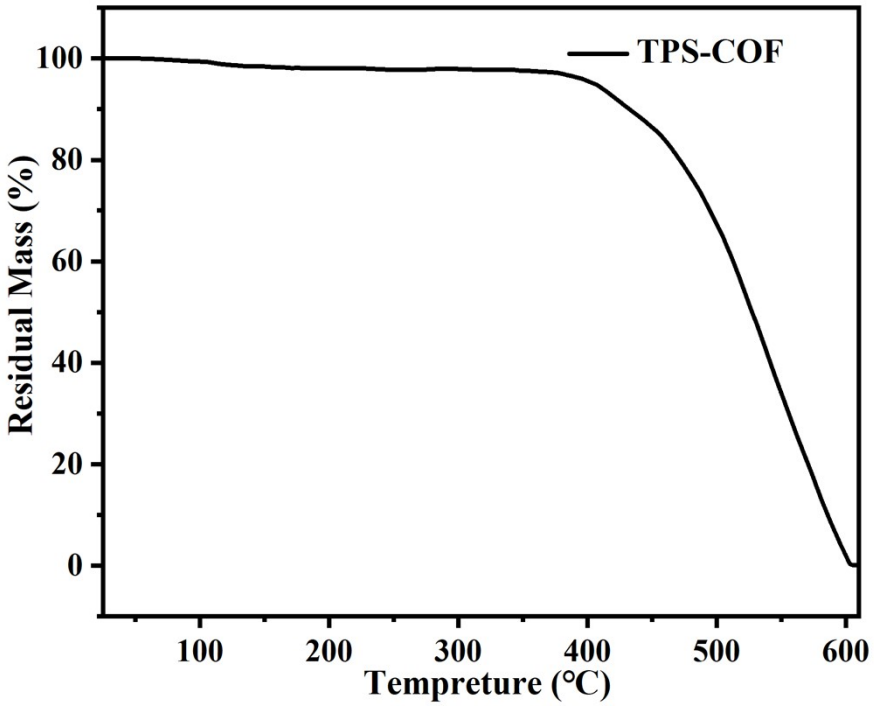

Fig. S5. TGA spectrum of TPS-COF (404°C, 5% weight loss).

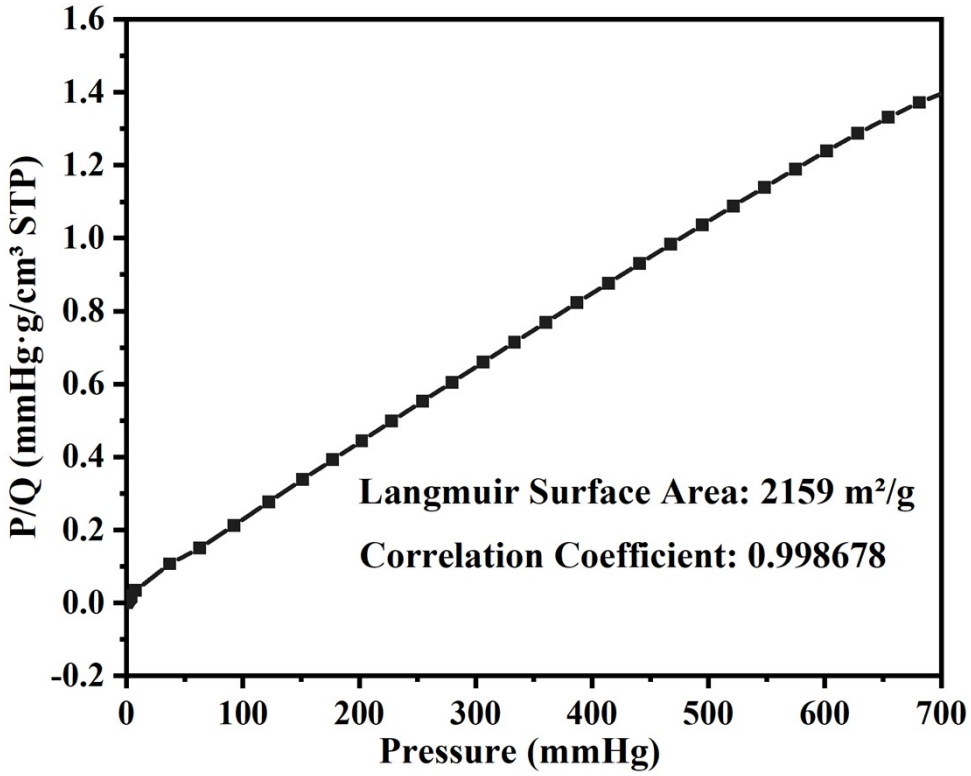

Fig. S6. Langmuir surface area of TPS-COF and its linear fit.

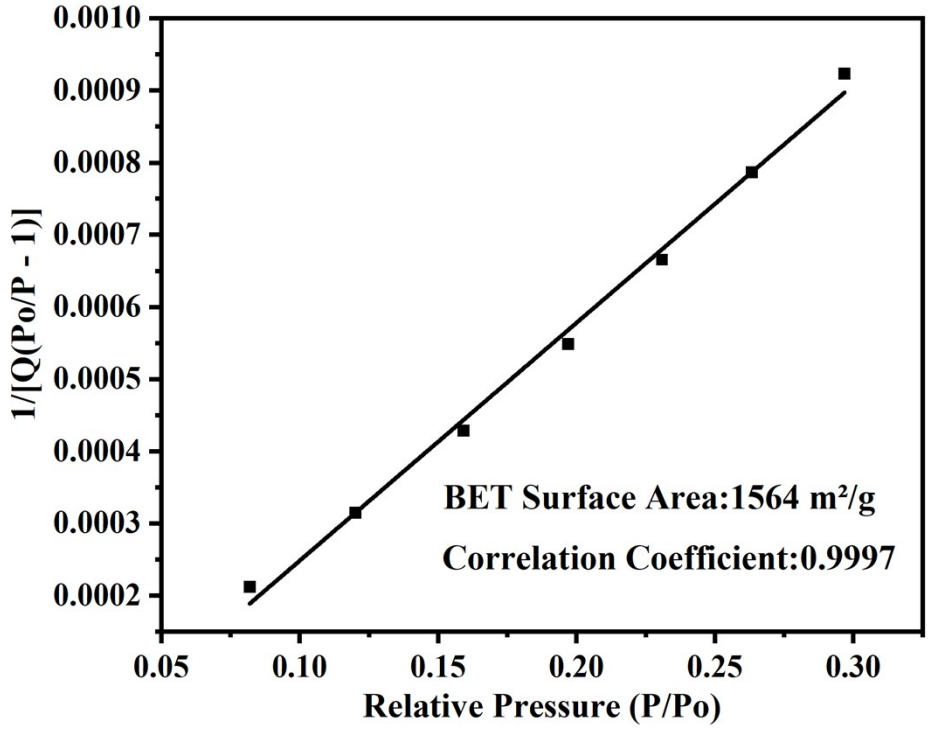

Fig. S7. BET surface area of TPS-COF and its linear fit.

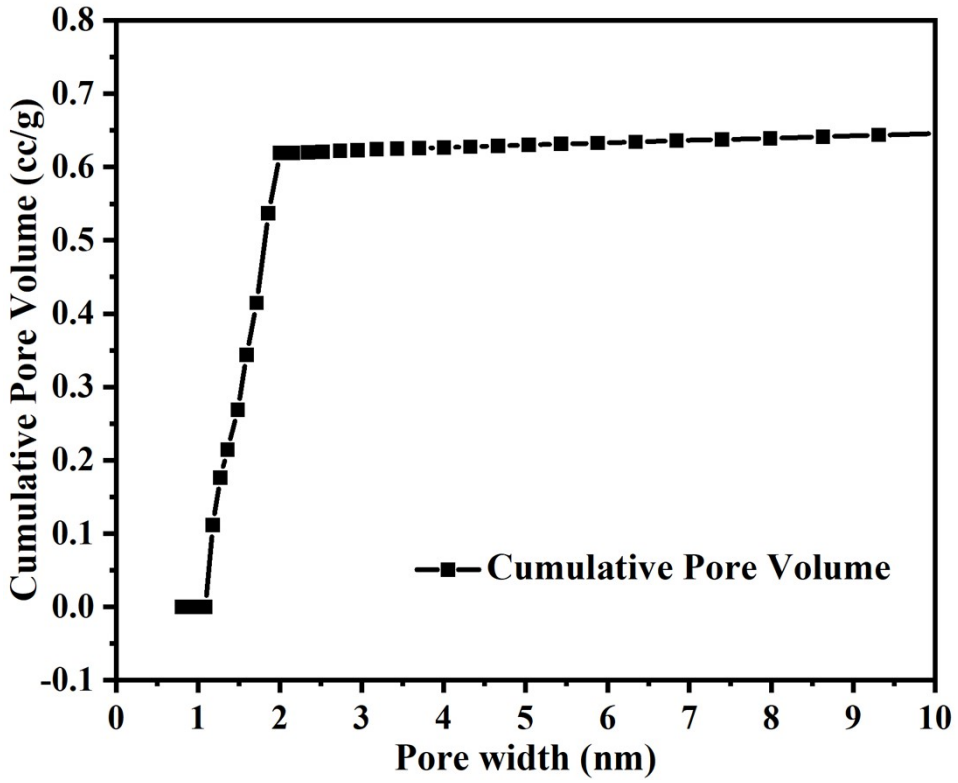

Fig. S8. Pore volume spectra of TPS-COF.

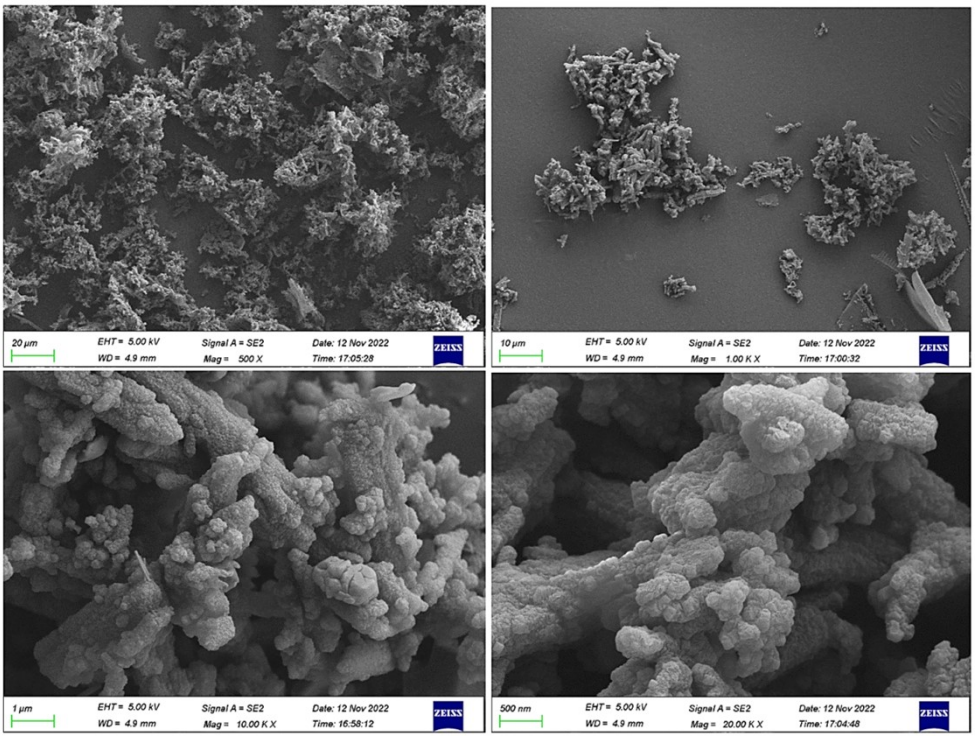

Fig. S9. SEM image of TPS-COF.

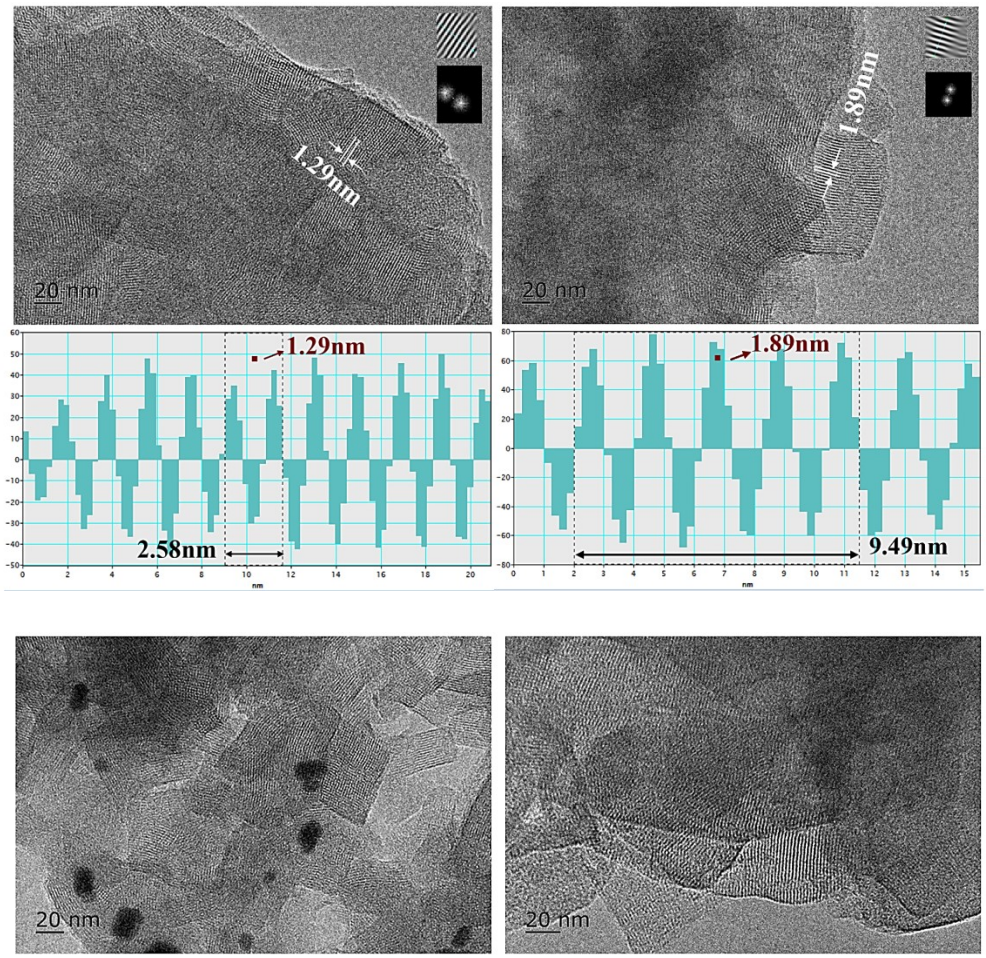

Fig. S10. HR-TEM image of TPS-COF.

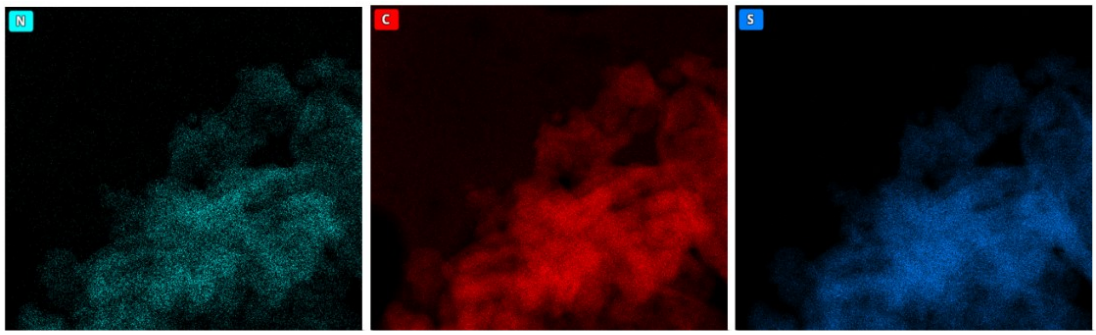

Fig. S11. EDS image of TPS-COF.

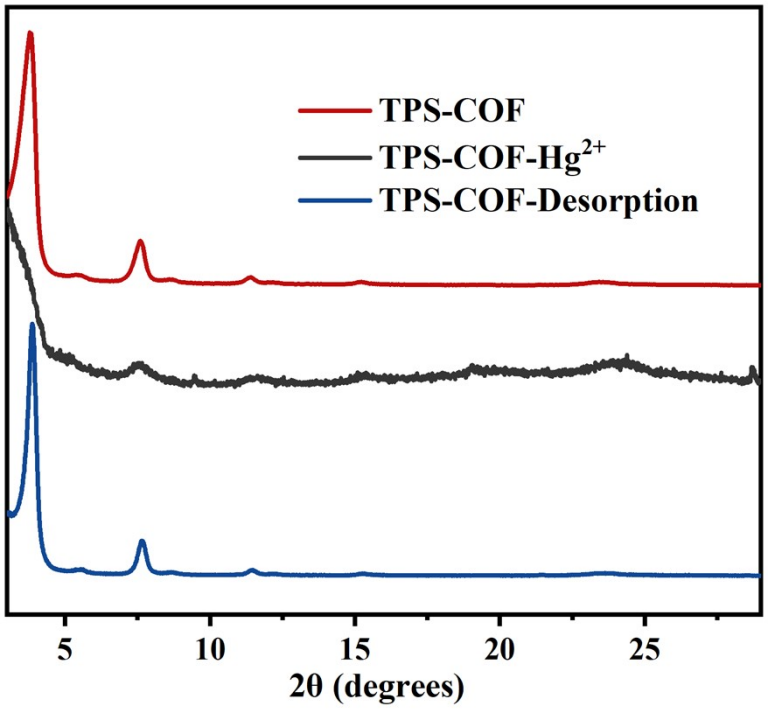

Fig. S12. PXRD comparison of TPS-COF and after adsorbed Hg^{2+}.

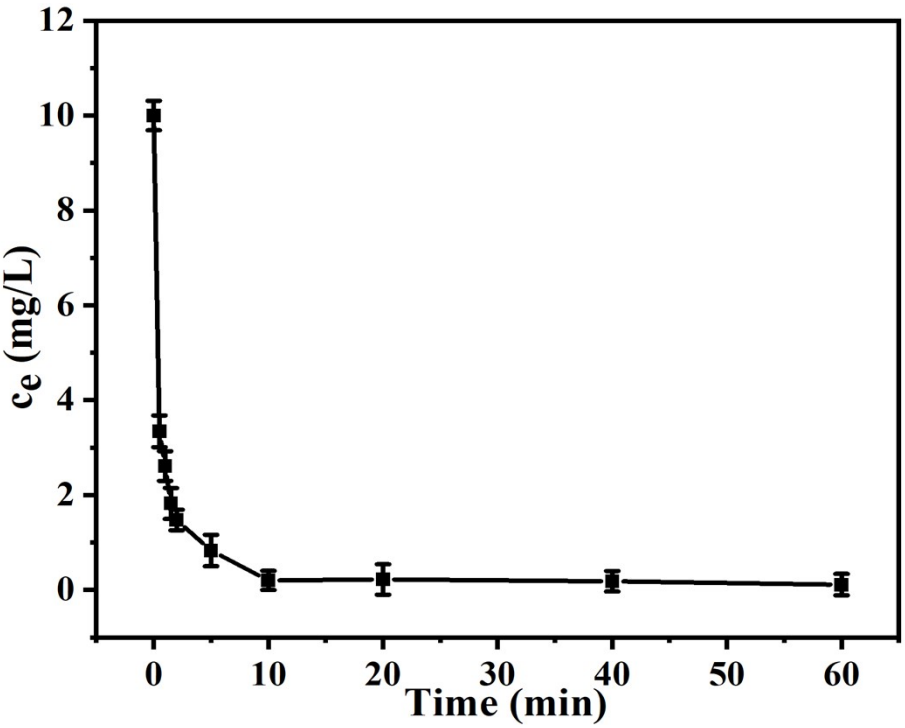

Fig. S13. Hg^{2+} uptake kinetics of TPS-COF.

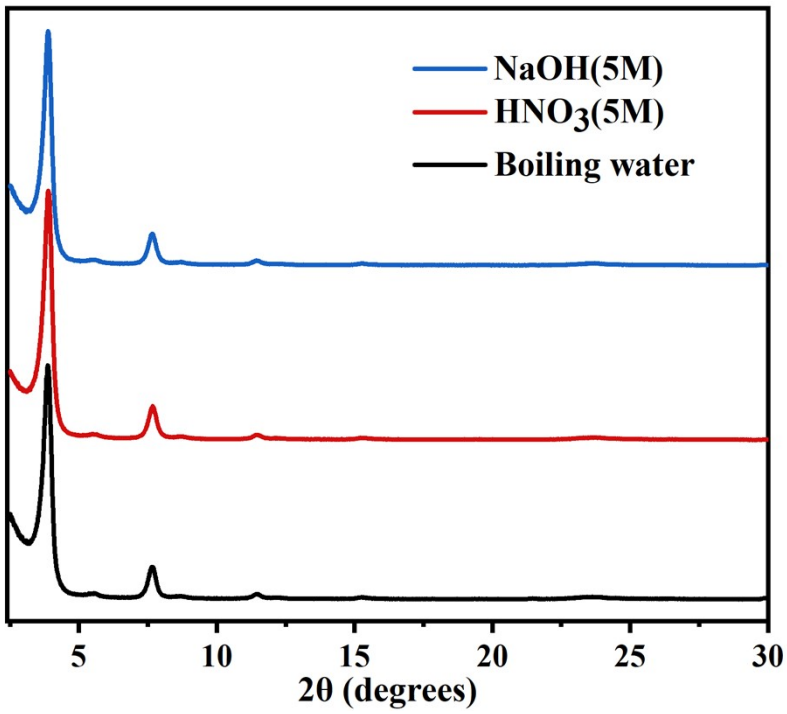

Fig. S14. PXRD of the stability of TPS-COF.

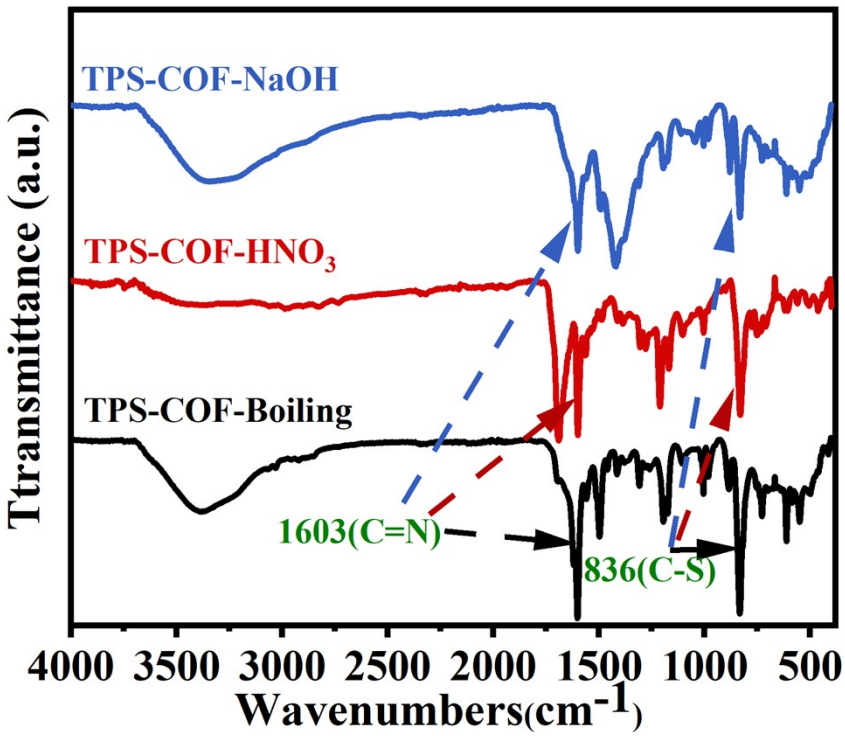

Fig. S15. FT-IR of the stability of TPS-COF.

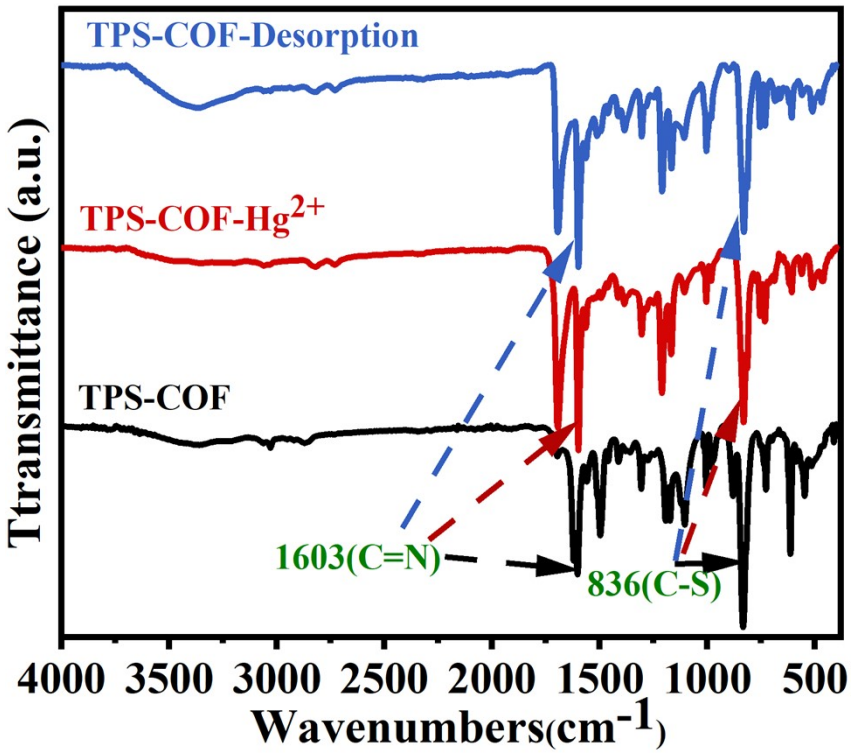

Fig. S16. FT-IR of the TPS-COF before and after the adsorption of Hg^{2+}.

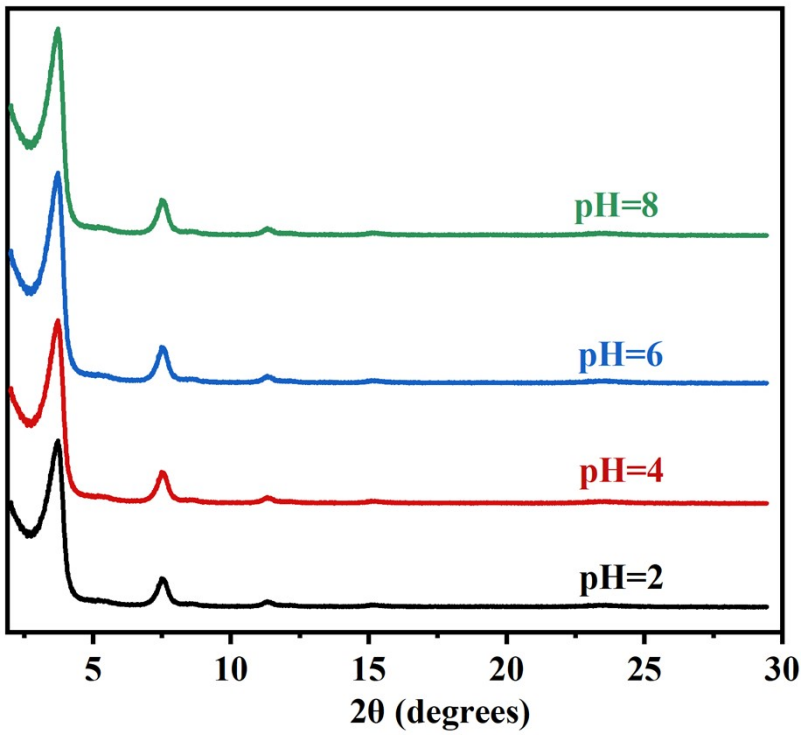

Fig. S17. PXRD of materials after regeneration at different pH environments.

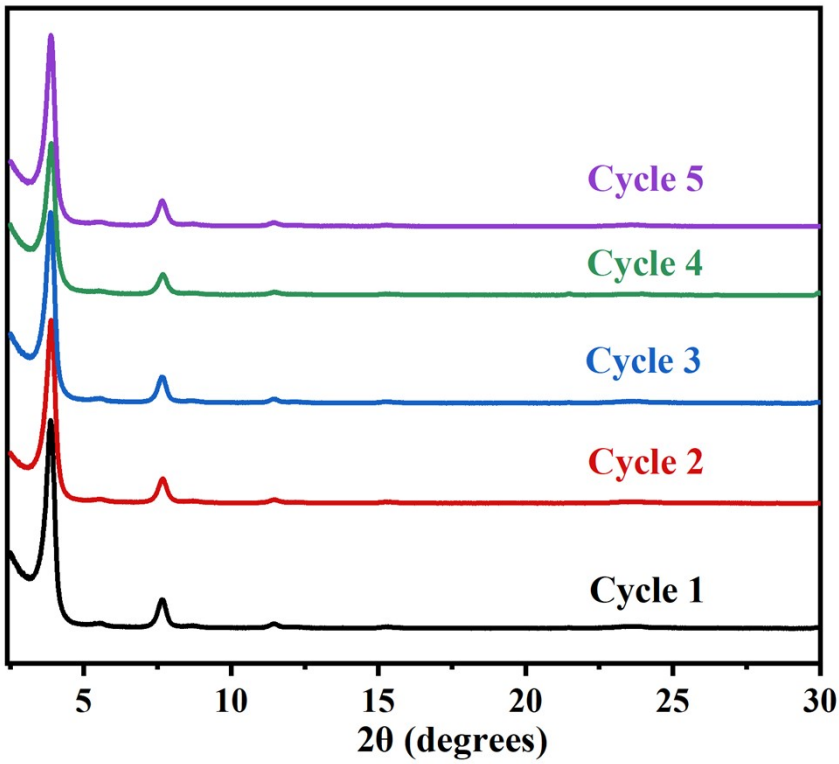

Fig. S18. PXRD of TPS-COF after 5 cycles of regeneration.

Section S5. References

[S1] Z. Ma, F. Liu, N. Liu, W. Liu and M. Tong, *J. Hazard. Mater.*, 2021, **405**, 124190.

[S2] L. Wang, H. Xu, Y. Qiu, X. Liu, W. Huang, N. Yan and Z. Qu, *J. Hazard. Mater.*, 2020, **389**, 121824.

[S3] L. Huang, R. Shen, R. Liu and Q. Shuai, *J. Hazard. Mater.*, 2020, **392**, 122320.

[S4] L. Merí-Bofí, S. Royuela, F. Zamora, M. L. Ruiz-González, J. L. Segura, R. Muñoz-Olivas and M. J. Mancheño, *J. Mater. Chem. A.*, 2017, **5**, 17973-17981.

[S5 N. Huang, L. Zhai, H. Xu and D. Jiang, *J. Am. Chem. Soc.*, 2017, **139**, 2428-2434.

[S6] X. Li, Y. Qi, G. Yue, Q. Wu, Y. Li, M. Zhang, X. Guo, X. Li, L. Ma and S. Li, *Green Chem.*, 2019, **21**, 649-657.

[S7] W. R. Cui, W. Jiang, C. R. Zhang, R. P. Liang, J. Liu and J. D. Qiu, *ACS Sustainable Chem. Eng.*, 2019, **8**, 445-451.

[S8] Q. Fu, T. Zhang, X. Sun, S. Zhang, G. I. N. Waterhouse, C. Sun, H. Li and S. Ai, *Chem. Eng. J.*, 2023, **454**, 140154.

[S9] Q. Sun, B. Aguila, J. Perman, L. D. Earl, C. W. Abney, Y. Cheng, H. Wei, N. Nguyen, L. Wojtas and S. Ma, *J. Am. Chem. Soc.*, 2017, **139**, 2786-2793.

[S10] W. Wang, M. Gong, D. Zhu, M. Vakili, Z. Gholami, H. Jiang, S. Zhou and H. Qu, *Environ. Sci. Ecotechnol.*, 2023, **14**, 100236.

[S11] M. Afshari, M. Dinari, K. Zargoosh and H. Moradi, *Ind. Eng. Chem. Res.*, 2020, **59**, 9116-9126.

[S12] Y. Li, T. Hu, R. Chen, R. Xiang, Q. Wang, Y. Zeng and C. He, *Chem. Eng. J.*, 2020, **398**, 125566.

[S13] H. L. Qian, M. S. Zhu, M. L. Du, X. Q. Ran and X. P. Yan, *J. Hazard. Mater.*, 2022, **427**, 128156.

[S14] C. Tang, Y. Qin, C. Ni and J. Zou, *ACS. Appl. Polym. Mater.*, 2022, **4**, 849-858.

[S15] R. Anbazhagan, R. Krishnamoorthi, S. Kumaresan, D. Thankachan, D. T. T. Van, J.-S. Wang and H.-C. Tsai, *React. Funct. Polym.*, 2021, **169**,105083.

[S16] S. Wang, Y. Xin, H. Hu, X. Su, J. Wu, Q. Yan, J. Qian, S. Xiao and Y. Gao, *RSC Adv.*, 2022, **12**, 35445-35451.

[S17] W.-T. Li, Y.-T. Zhuang, J.-Y. Wang, T. Yang, Y.-L. Yu, M.-L. Chen and J.-H. Wang, *ACS. Appl. Polym. Mater.*, 2019, **1**, 2797-2806.